

HIV gp41 six-helix bundle constructs induce rapid vesicle fusion at pH 3.5 and little fusion at pH 7.0: understanding pH dependence of protein aggregation, membrane binding, and electrostatics, and implications for HIV-host cell fusion

Kelly Sackett · Allan TerBush · David P. Weliky

Received: 13 October 2010/Revised: 26 November 2010/Accepted: 17 December 2010/Published online: 11 January 2011
© European Biophysical Societies' Association 2011

Abstract The HIV gp41 protein catalyzes fusion between HIV and target cell membranes. The fusion states of the gp41 ectodomain include early coiled-coil (CC) structure and final six-helix bundle (SHB) structure. The ectodomain has an additional N-terminal apolar fusion peptide (FP) sequence which binds to target cell membranes and plays a critical role in fusion. One approach to understanding gp41 function is study of vesicle fusion induced by constructs that encompass various regions of gp41. There are apparent conflicting literature reports of either rapid or no fusion of negatively charged vesicles by SHB constructs. These reports motivated the present study, which particularly focused on effects of pH because the earlier high and no fusion results were at pH 3.0 and 7.2, respectively. Constructs include “Hairpin,” which has SHB structure but lacks the FP, “FP-Hairpin” with FP + SHB, and “N70,” which contains the FP and part of the CC but does not have SHB structure. Aqueous solubility, membrane binding, and vesicle fusion function were measured at a series of pHs and much of the pH dependences of these properties were explained by protein charge. At pH 3.5, all constructs were positively charged, bound negatively charged vesicles, and

induced rapid fusion. At pH 7.0, N70 remained positively charged and induced rapid fusion, whereas Hairpin and FP-Hairpin were negatively charged and induced no fusion. Because viral entry occurs near pH 7 rather than pH 3, our results are consistent with fusogenic function of early CC gp41 and with fusion arrest by final SHB gp41.

Keywords HIV · gp41 · Membrane fusion · Six-helix bundle · Pre-hairpin intermediate · pH

Abbreviations

Chol	Cholesterol
CHR	C-terminal heptad repeat
FP	Fusion peptide
LUV	Large unilamellar vesicle
MPER	Membrane-proximal external region
NCL	Native chemical ligation
NHR	N-terminal heptad repeat
N-dansyl-DOPE	<i>N</i> -(5-dimethylamino-1-naphthalenesulfonyl) (ammonium salt) dioleoylphosphatidylethanolamine
N-NBD-DPPE	<i>N</i> -(7-nitro-2,1,3-benzoxadiazol-4-yl) (ammonium salt) dipalmitoylphosphatidylethanolamine
N-Rh-DPPE	<i>N</i> -(lissamine rhodamine B sulfonyl) (ammonium salt) dipalmitoylphosphatidylethanolamine
N-PHI	N-terminal half of the pre-hairpin intermediate
PC	Phosphatidylcholine
PE	Phosphatidylethanolamine
PG	Phosphatidylglycerol
PHI	Pre-hairpin intermediate
POPC	1-Palmitoyl-2-oleoyl- <i>sn</i> -glycero-3-phosphocholine

Membrane-active peptides: 455th WE-Heraeus Seminar and AMP 2010 Workshop.

K. Sackett · D. P. Weliky (✉)
Department of Chemistry, Michigan State University,
East Lansing, MI 48824, USA
e-mail: weliky@chemistry.msu.edu

A. TerBush
Department of Biochemistry and Molecular Biology,
Michigan State University, East Lansing, MI 48824, USA

POPG	1-Palmitoyl-2-oleoyl- <i>sn</i> -glycero-3-[phospho- <i>rac</i> -(1-glycerol)] (sodium salt)
PS	Phosphatidylserine
RP-HPLC	Reverse phase-high performance liquid chromatography
SHB	Six-helix bundle
Sph	Sphingomyelin
TCEP	Tris(2-carboxyethyl) phosphine hydrochloride

Introduction

The HIV transmembrane protein gp41 directs fusion between the viral envelope and target cell membranes as an initial step in host cell infection (Figs. 1, 2a). During fusion, gp41 adopts distinct conformations, and there is fundamental interest in the mechanism by which specific structures and/or structural changes of gp41 direct membrane fusion (White et al. 2008). The ~180-residue gp41 ectodomain lies outside the virus and begins with the apolar fusion peptide (FP) region followed by N-heptad repeat (NHR), loop, and C-heptad repeat (CHR) (Fig. 2a). Gp41 is trimeric, and early fusion-active conformation termed the pre-hairpin intermediate (PHI) (Fig. 1b) has an extended ectodomain with parallel coiled-coil assembly of the NHR (Bewley et al. 2002; Furuta et al. 1998; Jones et al. 1998). It is generally written that the FP in the PHI is bound to the target cell membrane although, to our knowledge, this has not been experimentally verified (Durell et al. 1997; White et al. 2008). Hydrophobic interaction between the NHRs and CHRs results in collapse to a final hyperthermostable and compact six-helix bundle

(SHB) structure (Fig. 1c) (Caffrey et al. 1998; Tan et al. 1997; White et al. 2008).

Virus–cell membrane fusion is generally accepted to occur through the following sequential steps: (1) mixing of lipids between the two membrane bilayers; (2) formation of a hemifusion intermediate with retention of distinct virus and cell compartments separated by a single bilayer “diaphragm”; (3) breaking the diaphragm to make a fusion pore with creation of a single continuous membrane enclosing the virus and cell compartments; and (4) enlargement of the fusion pore and complete mixing of virus and cell contents (Chernomordik et al. 2006). Although these membrane fusion steps occur contemporaneously with the gp41 structural changes pictured in Fig. 1, it is not yet clear how specific gp41 structures or structural changes catalyze particular fusion steps or are time-correlated with these steps (Markosyan et al. 2003). One widely presented idea is that no membrane fusion steps occur prior to folding from PHI to SHB structure and that this folding initiates fusion by bringing virus and cell membranes close together. (Chan and Kim 1998; Weissenhorn et al. 1997). For this model, fusion catalysis occurs because much of the free energy released by PHI → SHB folding is transformed into free energy of activation of membrane fusion. To our knowledge, there are no clear experimental data which support this model. An alternative hypothesis is that PHI structure correlates with lipid mixing and hemifusion and that SHB formation is coincident with creation of small, stable fusion pores. There are some gp41-mediated cell fusion data which support this model (Markosyan et al. 2003).

Several constructs encompassing various regions of gp41 catalyze vesicle fusion as assayed by inter-vesicle lipid mixing, and these data provide useful information to understand gp41-mediated membrane fusion. A variety of membrane compositions have been used in these assays,

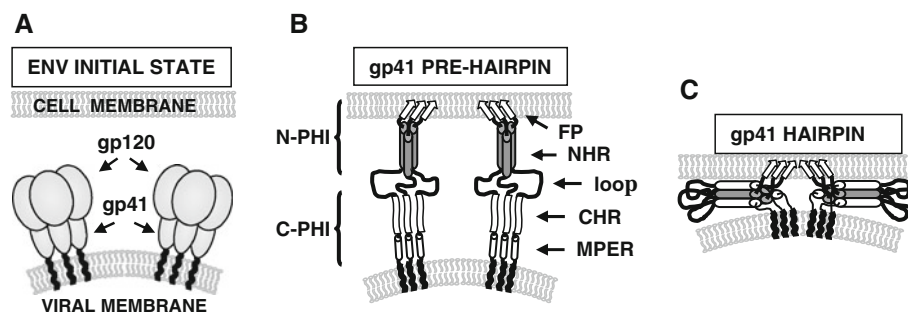
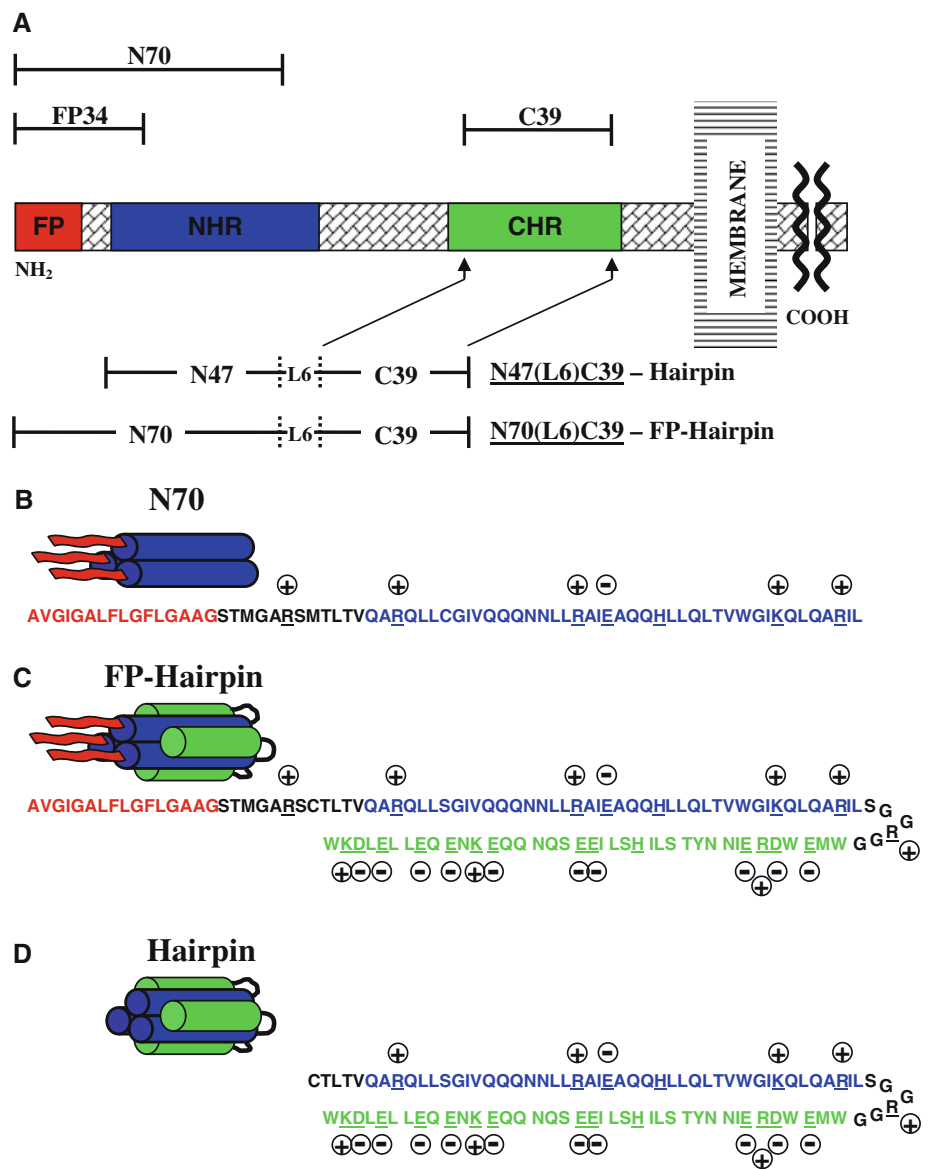


Fig. 1a–c HIV fusion model. **a** On naïve virions, trimeric gp41 is initially sequestered by three viral gp120 surface subunits (Center et al. 2002). **b, c** Following binding by gp120 with specific target cell receptors, gp41 becomes activated and undergoes conformational change, interacts with the target cell membrane, and directs membrane fusion (Furuta et al. 1998; Jones et al. 1998; Markosyan et al. 2003). Gp120 is omitted from **b** and **c** in order to focus on gp41 organization. To date, there are high-resolution structures for the SHB

structure of **c** and high-resolution structures for FP in membranes and in detergent which show both β sheet and helical conformations (Jaroniec et al. 2005; Li and Tamm 2007; Pereira et al. 1997; Qiang et al. 2008; Reichert et al. 2007; White et al. 2008). There are conflicting reports about the fractions of specific parallel and antiparallel β sheet registries (Sackett and Shai 2005; Yang and Weliky 2003)

Fig. 2 a Schematic of the HIV gp41 ectodomain with functional regions designated by colored boxes. Above and below in brackets are gp41 constructs. **b–d** Structural representation of N70, FP-Hairpin (N70(L6)C39), and Hairpin (N47(L6)C39), respectively, in aqueous solution, with primary sequence color-coded to match functional regions in **a**. The alignment of the NHR and CHR sequences approximately reflects their alignment in crystal structures of HIV gp41 in SHB conformation (Chan et al. 1997; Weissenhorn et al. 1997). Basic and acidic amino acids (other than histidine) are *underlined* and marked by an adjacent *circled plus* or *minus sign*, respectively. At most pHs, the N-terminus of each molecule carries a positive charge while the C-termini of Hairpin and FP-Hairpin carry a negative charge. N70 has uncharged C-terminal amidation



and reference compositions include those from membranes of host cells of HIV or from HIV itself. A reasonable model of the lipid headgroup + cholesterol composition of the host cell is denoted “LM3” and has phosphatidylcholine (PC):phosphatidylethanolamine (PE):phosphatidylserine (PS):sphingomyelin (Sph):phosphatidylinositol (PI):cholesterol (Chol) in a 33:17:7:7:3:33 mol ratio (Aloia et al. 1993; Brugger et al. 2006; Yang et al. 2001). A model composition for HIV is PC:Sph:PE:PS:Chol in 15:15:15:10:45 mol ratio. Because the FP is thought to initially bind to the host cell membrane, studies of FP-containing constructs have typically focused on LM3-type compositions.

There have also been studies of gp41 construct-induced fusion of vesicles with simpler compositions, most notably PC:PG:Chol in 0.53:0.13:0.34 (8:2:5) mol ratio (Sackett

et al. 2009, 2010). This composition reflects the respective large and small fractions of lipids with choline and negatively charged headgroups in LM3 as well as the significant fraction of cholesterol in both cellular and HIV membranes (Aloia et al. 1993; Brugger et al. 2006). We note that a 4:1 PC:PG mol ratio has been commonly used in biophysical studies of viral fusion proteins and that negatively charged lipids are found in the outer leaflet of the HIV membrane (Aloia et al. 1993; Callahan et al. 2003; Han et al. 2001; Macosko et al. 1997; Nguyen and Hildreth 2000). The relevance of the PC:PG:Chol and PC:PG compositions has been evidenced by the following: (1) for a particular gp41 construct, the rate and extent of fusion of vesicles with the PC:PG:Chol or PC:PG composition is typically similar to that observed with the more complex LM3 composition; and (2) fusogenicity trends among different gp41

constructs are observed with LM3, PC:PG:Chol, or PC:PG vesicles (Sackett et al. 2010; Yang et al. 2004b). The present study focuses on fusion in the pH 3–7 range, and PG rather than PS was used in part because the apparent pK_a of PG in vesicles is in the 1–3 range, whereas the pK_a of PS is in the 3–5 range (Tocanne and Teissie 1990; Tsui et al. 1986; Winiski et al. 1986). Relative to vesicles with PS, a much higher degree of negative vesicle charge will be maintained at low pH for vesicles with PG, and the pH dependence of protein-vesicle electrostatic energy can be primarily understood in terms of changes in protein charge.

N70 has been a commonly studied gp41 construct and is the 70 N-terminal gp41 residues, which includes the FP and most of the NHR (Fig. 2) (Sackett et al. 2009; Sackett and Shai 2002). N70 serves as a model of the N-terminal half of the PHI conformation (N-PHI), and at pH 7.2 induced rapid fusion between vesicles with the 8:2:5 POPC:POPG:Chol composition. Extensive N70-induced fusion has also been reported for vesicles with a fraction of either negatively charged PS or PG lipid (Korazim et al. 2006; Sackett et al. 2009, 2010; Sackett and Shai 2003). The construct “FP-Hairpin” contained the FP, NHR, short non-native loop, and CHR and has hyperthermostable ($T_{melt} \approx 110^\circ\text{C}$) SHB structure (Fig. 2) (Sackett et al. 2009, 2010). In striking contrast to N70, FP-Hairpin induced no vesicle fusion at pH 7.2, and addition of FP-Hairpin stopped vesicle fusion initiated by shorter constructs such as FP34 (Fig. 2a). However, there was another literature report that SHB constructs either with or without the FP induced extensive vesicle fusion at pH 3.0 (Lev et al. 2009). Such fusion was observed for vesicles with 45 mol% negatively charged lipid but not for vesicles without negatively charged lipid, although we note that a third group has reported significant fusion for neutral vesicles at pH 7.5 with an FP + SHB construct (Cheng et al. 2010). These different results motivated the present study to examine the effect of pH on vesicle fusion induced by N70 and FP-Hairpin. Experiments were also carried out on the NHR + loop + CHR “Hairpin” construct with known SHB structure in order to (1) distinguish the contributions to fusogenicity from the FP and SHB regions as well as their pH dependences; and (2) compare to the earlier report of high fusogenicity at pH 3.0 from SHB constructs with or without the FP (Sackett et al. 2009, 2010). The pH dependences of aqueous solubility and membrane binding of each construct were also examined as these properties might be correlated to fusogenicity. For example, aggregation and/or lack of membrane binding might be reasons for low fusogenicity.

This pH-dependent study was motivated by fundamental biophysical interest and the desire to understand apparently very different results from the literature. We note that HIV/host cell fusion likely occurs at physiologic pH ≈ 7 as there is significant evidence for fusion between the virus and plasma membranes (Grewe et al. 1990; Stein et al.

1987). Endocytosis of HIV has also been observed, but any fusion between HIV and endocytic membranes likely occurs in neutral rather than acidified (pH ≈ 5.5) endosomes (McClure et al. 1988; Miyauchi et al. 2009). The larger goal of our work is to elucidate specific membrane fusion functional roles of intermediate and final gp41 conformations such as those displayed in Fig. 1.

Materials and methods

Materials

Boc and Fmoc amino acids, Boc MBHA resin, and Fmoc rink amide MBHA resin were purchased from Novabiochem. *S*-Trityl- β -mercaptopropionic acid was purchased from Peptides International. Di-*tert*-butyl-dicarbonate, Tris(2-carboxyethyl) phosphine hydrochloride (TCEP), and Triton X-100 were purchased from Sigma. *N*-(7-nitro-2,1,3-benzoxadiazol-4-yl) (ammonium salt) dipalmitoylphosphatidylethanolamine (*N*-NBD-DPPE), *N*-(lissamine rhodamine B sulfonyl) (ammonium salt) dipalmitoylphosphatidylethanolamine (*N*-Rh-DPPE), *N*-(5-dimethylamino-1-naphthalenesulfonyl) (ammonium salt) dioleoylphosphatidylethanolamine (*N*-dansyl-DOPE), 1-palmitoyl-2-oleoyl-*sn*-glycero-3-phosphocholine (POPC), 1-palmitoyl-2-oleoyl-*sn*-glycero-3-[phospho-*rac*-(1-glycerol)] (sodium salt) (POPG), and cholesterol (Chol) were purchased from Avanti Polar Lipids. All other reagents were of analytical grade.

Peptide and protein sequences

The sequences in Fig. 2b–d are from the Envelope protein of the HXB2 strain of HIV-1. Residue 512 of Envelope corresponds to residue 1 of gp41.

Peptide synthesis

Peptides included FP34(linker), 512–545-(thioester); FP23(linker), 512–534(S534A)-(thioester); and N36(S546C), 546–581 (Fig. 2). Peptides were synthesized as described previously and purified to >95% purity by reverse phase-high performance liquid chromatography (RP-HPLC) on C18 or C4 semi-preparative columns using a linear gradient between water/0.1% trifluoroacetic acid and 10% water/90% acetonitrile/0.1% trifluoroacetic acid (Sackett and Shai 2002; Sackett et al. 2006). Purified peptides were lyophilized and stored at -20°C under argon. Mass spectroscopy was used to confirm the identity of each purified peptide with respective expected and observed masses of 3,580.0 and 3,580.2 Da for FP34(linker), 2,195.5 and 2,194.4 Da for FP23(linker), and 4,138.8 and 4,138.7 Da for N36(S546C).

Protein expression

The Hairpin construct with NHR + loop + CHR and SHB structure was composed of Envelope residues 535(M535C) to 581 (gp41 residues 24–70) followed by a short non-native SGGRGG loop and then residues 628–666 (gp41 residues 117–155) (Fig. 2). Hairpin was expressed and purified as described previously (Curtis-Fisk et al. 2008; Sackett et al. 2009). Expression was done in BL-21 cells using the T7 expression system, and following bacteria growth, induction, and protein expression, the centrifuged cell pellet was lysed with glacial acetic acid. After centrifugation, the supernatant was dialyzed against trifluoroacetic acid:water (1:2,000 v/v) with 150 μ M dithiothreitol reducing agent, and then filtered and concentrated. Hairpin was purified to >95% homogeneity by RP-HPLC using a C18 preparative column, lyophilized, and stored under argon at -20°C . Mass spectroscopy confirmed Hairpin identity (10,724.1 Da expected mass and 10,724.5 Da observed mass), and quantification was based on A_{280} using $\epsilon = 23,490 \text{ M}^{-1} \text{ cm}^{-1}$.

Native chemical ligation

N70 was prepared by ligating FP34(linker) with N36(S546C) as described previously (Sackett et al. 2006). The FP + SHB construct (FP-Hairpin) was prepared by ligating FP23(linker) with purified Hairpin at ambient temperature in a solution containing 8 M guanidinium chloride and 30 mM 4-mercaptophenylacetic acid (Johnson and Kent 2006; Sackett et al. 2009). Ligation reactions were purified by RP-HPLC using a C4 semi-preparative column with N70 or FP-Hairpin eluting as a well-separated single peak that was identified by mass spectroscopy. FP-Hairpin was dialyzed into 10 mM formate with 200 μ M TCEP reducing agent at pH 3.0 and stored at 4°C , while N70 was lyophilized and stored under argon at -20°C . For either the N70 or FP-Hairpin ligations, the guanidinium chloride denaturant eluted in the HPLC void volume during purification and a subsequent HPLC of the purified product showed no guanidinium chloride contaminant. Mass spectroscopy confirmed FP-Hairpin and N70 identity with respective expected and observed masses of 7,500.9 and 7,500.5 Da for N70 and 12,814.6 and 12,816.0 Da for FP-Hairpin. Quantification was based on A_{280} using $\epsilon = 5,500$ and $23,490 \text{ M}^{-1} \text{ cm}^{-1}$ for N70 and FP-Hairpin, respectively.

Protein aqueous solubility

A 40 μ M solution of each gp41 construct was prepared in either 10 mM formate with 200 μ M TCEP at pH = 3.0 or 25 mM citrate with 200 μ M TCEP at pH \approx 3.5. Under

constant stirring, pH was either increased or decreased with aliquots of NaOH or HCl solution, respectively. Sample aliquots were removed at each titration point, centrifuged for 5 min at 14,000 g, and soluble concentration was determined by A_{280} of the supernatant. The lower detection limit for A_{280} was 0.03 and corresponded to a minimum detectable concentration of 1.5 μ M for Hairpin and FP-Hairpin and 5.5 μ M for N70. When $A_{280} \geq 0.1$, spectral appearance between 200 and 350 nm was typical for a protein with tryptophan(s) with absorbance maximum and shoulder at 280 and 290 nm, respectively.

Protein binding to membranes

Protein binding to vesicles was qualitatively measured from 525 nm fluorescence of dansyl headgroup-labeled lipids which had been excited by energy transfer from protein tryptophans that were excited by 280 nm radiation. The Förster distance of the tryptophan-dansyl pair is $\sim 22 \text{ \AA}$, which indicates that distances up to $\sim 30 \text{ \AA}$ result in measurable energy transfer (Wu and Brand 1994). Large unilamellar vesicles (LUVs) were prepared by extrusion of lipid films through filters with 100 nm pore diameters (Yang et al. 2004b). The composition of the vesicles was POPC:POPG:*N*-dansyl-DOPE:Chol in a 7.5:2.0:0.5:5.0 mol ratio. The vesicles were extruded with [total lipid + cholesterol] $\approx 10 \text{ mM}$, and the buffer was 25 mM *N*-(2-hydroxyethyl) piperazine-*N'*-2-ethanesulfonic acid (HEPES) at pH 7.4. Vesicles were diluted to [total lipid + cholesterol] $\approx 230 \mu\text{M}$ in 25 mM citrate buffer with final pH = 3.5, 4.5, 5.0, or 7.0. The vesicle solution was transferred to the fluorimeter (Photon Technology International model 810) and was contained in a glass cuvette at 37°C with constant stirring. The excitation wavelength was the absorption maximum of tryptophan = 280 nm, and the fluorescence wavelength was the emission maximum of the dansyl vesicles = 525 nm. Fluorescence was detected at 90° relative to the incident beam, and 5 nm slit widths were used for both excitation and emission. Baseline fluorescence of the vesicle solution was first measured for 20 s, protein solution was then added, and fluorescence was measured for an additional 10 min with steady-state fluorescence usually reached within 30 s. There was typical variation of <5% in absolute fluorescence among different repetitions of the assay. Each protein stock solution had [protein] = 40 μ M in 10 mM formate, 200 μ M TCEP pH 3.0. For N70, 60 μ L of stock solution was added to 1.2 mL vesicle solution so that final [N70] = 2 μ M. For Hairpin and FP-Hairpin, 30 μ L of stock solution was added so that final [Hairpin] or [FP-Hairpin] = 1 μ M. The pH of the vesicle + protein solution was the same as the pH of the initial vesicle solution.

Protein-induced vesicle fusion

Protein-induced vesicle fusion was detected by mixing of lipids between the fusing vesicles. The particular assay was the increase in fluorescence observed when a vesicle “labeled” with small fractions of fluorescent and quenching lipids fuses with a vesicle without these lipids (Struck et al. 1981). The fluorescence increase reflected the larger average fluorophore-quencher distance in the fused vesicle. The procedure for vesicle preparation was similar to that described for the membrane binding experiments with [total lipid + cholesterol] \approx 230 μ M in a 25 mM citrate buffer with pH = 3.5, 4.0, 4.2, 4.6, 5.0, 5.5, 6.0, 6.5, or 7.0. Ninety percent of the vesicles were “unlabeled” and contained POPC:POPG:Chol (8:2:5); and ten percent were “labeled” with an additional 2 mol% *N*-NBD-DPPE fluorescent lipid and 2 mol% *N*-Rh-DPPE quenching lipid. Fluorescence was done in a manner similar to that of the binding experiments except with excitation and fluorescence wavelengths of 467 and 530 nm, which were the peak absorption and emission wavelengths of the *N*-NBD-DPPE fluorescent lipid. In addition, the time-resolved “percent lipid mixing” or $M(t)$ was calculated from the time-resolved fluorescence change $\Delta F(t)$ measured after addition of protein. The maximum fluorescence change ΔF_{\max} was measured after subsequent addition of 12 μ L of 10% Triton X-100 detergent. This solubilized the lipids and cholesterol with resultant very large average fluorophore-quencher distance. The $M(t) = \Delta F(t)/\Delta F_{\max} \times 100$ with typical variation of <5% in the long-time value of $M(t)$ among different repetitions of the assay. The $\Delta F(t)$ and ΔF_{\max} were corrected for the fluorophore dilution from the small increase in volume from the added protein or detergent solution.

An assay variant that probed pH-triggered vesicle fusion was also done. Baseline fluorescence was measured for the vesicle-only solution at pH 7.0, $\Delta F(t)$ was measured following addition of protein and then measured after subsequent addition of an HCl aliquot which reduced the pH to 3.3. The effect of lowered pH on vesicle fluorescence was probed by another assay variant in which the HCl aliquot was added first with subsequent addition of the protein.

Results and discussion

pH-dependent aqueous solubility

The vesicle fusion assays were done by addition of an aqueous protein solution to a membrane vesicle solution. Binding of the protein to the vesicle is likely a prerequisite for fusion. However, in aqueous solution, the gp41 constructs often have exposed apolar regions such as the FP,

and under some solution conditions these regions have been shown to form large aggregates (Yang et al. 2001, 2004a). Such aggregation might compete and/or interfere with membrane binding and/or fusion. In order to understand the possible contribution of pH-dependent protein aggregation to pH-dependent fusion, measurements were made of the aqueous solubilities of N70, Hairpin, and FP-Hairpin at different pHs (Fig. 3). By the centrifugation assay described in the “Materials and methods” section, all constructs at the initial pH of 3.0–3.5 were fully soluble for [protein] = 40 μ M \equiv 100% solubility. For comparable solution conditions, a significant fraction of N70 molecules have been shown to be trimers with coiled-coil NHR assembly, while the NHR + loop + CHR region of Hairpin and FP-Hairpin have trimeric SHB structure (Fig. 2b–d) (Sackett et al. 2006, 2009, 2010).

Figure 3a (black circles) shows that N70 remains fully soluble up to pH \approx 8 with decreasing solubility in the pH 8–10 range and \sim 0% solubility in the pH 10–12 range. Both Hairpin (blue circles) and FP-Hairpin (red circles) are soluble to pH \approx 4 with decreasing solubility in the pH 4–5 range and \sim 0% solubility in the pH 5–6 range. FP-Hairpin remains largely insoluble at higher pHs whereas Hairpin returns to 100% solubility in the pH 6–7 range and retains this solubility to pH 10 (Fig. 3b). This panel also shows that Hairpin solubility profiles are very similar in formate and citrate solutions, where the latter buffers over a greater pH range. The aggregation of Hairpin in the pH 4–6 range is reversible as evidenced by return to 100% solubility when the pH was increased to 7 or decreased to 3 (Fig. 3c). It is therefore likely that there are folded SHB trimers in the aggregates, which is consistent with the $T_{\text{melt}} \approx 110^\circ\text{C}$ for SHB trimers, i.e., hyperthermostability. FP-Hairpin aggregation was similarly reversible (Fig. 3d).

Much of the pH dependences of the solubilities of the three constructs can be understood in terms of their pIs. We first consider Hairpin whose sequence (Fig. 2d) shows a larger number of acidic than basic residues and whose pI = 5.3 was calculated from a model of independent ionizable groups (e.g., $-\text{COOH}$) whose $\text{pK}_{\text{a,s}}$ are the same as those of single amino acids (Bjellqvist et al. 1993; Gastegger et al. 2005). For pH = pI, we expect uncharged Hairpin, and as the pH is decreased (increased) from pI, Hairpin attains greater positive (negative) charge. Aggregation is disfavored by inter-protein electrostatic repulsion, and we therefore expect highest Hairpin solubility for pHs that are very different than the pI, as is experimentally observed (Fig. 3). The high and low solubilities of N70 for the pH = 3–8 and 10–12 ranges, respectively, can be similarly understood by its calculated pI = 11.5. The high and low solubilities of FP-Hairpin in the pH 3–4 and 4–7 ranges correlate with its calculated pI = 5.6. The continued low solubility at higher pHs for FP-Hairpin is likely

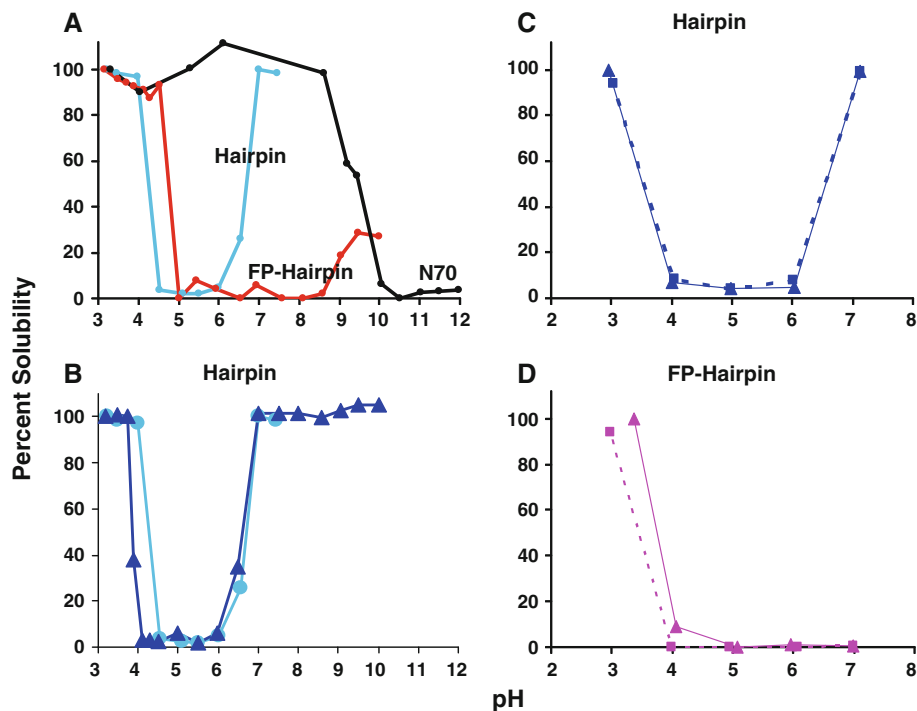


Fig. 3a–d The pH-dependent solubility of HIV gp41 constructs where 100% solubility corresponds to 40 μ M. Each construct was initially completely dissolved at 40 μ M at pH \approx 3.0, and the pH was incrementally increased with concentrated NaOH. For **c** and **d**, this was followed by reverse titration to lower pH using concentrated HCl. For all panels, lines are drawn between data points. **a** Solubility of N70 (black), FP-Hairpin (red), and Hairpin (light blue) in 10 mM formate solution. **b** Solubility of Hairpin in 10 mM formate (light

blue circles) or 25 mM citrate solution (dark blue triangles). **c** Hairpin and **d** FP-Hairpin solubility in 25 mM citrate buffer where triangles correspond to titration to higher pH and squares correspond to subsequent titration to lower pH. For **a**, comparison of experimental replicates resulted in the following estimated uncertainties for each datum: Hairpin and FP-Hairpin, $\pm 4\%$; N70, $\pm 10\%$. The uncertainties of the N70 data were larger because of the smaller N70 extinction coefficient and absorbances

due to the relatively small negative protein charge at pHs between the pI and the pK_a of lysine. The resultant small inter-trimer electrostatic repulsion is insufficient to counteract the hydrophobicity of the FP segments.

pH-dependent membrane binding

Protein binding to vesicles merits investigation because this binding is likely a requirement of protein-induced vesicle fusion. Figure 4a1, b1, c1 displays the fluorescence of the dansyl-labeled vesicles in the absence (time < 20 s) and presence (time > 20 s) of protein. Binding of the protein to vesicles is indicated by increased vesicle fluorescence due to energy transfer from excited tryptophan(s) in the protein. It was not possible to determine a binding constant because only a single protein and single vesicle concentration were used. Relative to only vesicles, N70 + vesicles had greatly increased fluorescence for pHs in the 3.5–7.0 range (Fig. 4c1), which supports substantial N70 binding to the vesicles for this pH range. Similarly at pH 3.5, addition of Hairpin caused a substantial jump in vesicle dansyl fluorescence, and there was a monotonic decrease in the fluorescence change as pH was raised with

change ≈ 0 at pH 7.0 (Fig. 4a1). These data support substantial binding of Hairpin to vesicles at pH 3.5 and a decrease in binding as pH is raised with no binding at pH 7.0. At pH 3.5, FP-Hairpin also bound vesicles significantly, and the binding appeared to decrease somewhat with higher pH, but unlike Hairpin, there was still substantial binding at pH 7.0 (Fig. 4b1). This retention of binding is likely due to the apolar FP region which by itself is known to bind to membranes at pH 7.0 (Qiang et al. 2009).

Hairpin lacks the FP, and the pH dependence of its binding can be understood in terms of electrostatic interactions with the negatively charged vesicles whose composition was designed to model the average fraction of negatively charged lipids of host cell membranes. Given the pI = 5.3 (consistent with the pH dependence of solubility, Fig. 3b), Hairpin would be positively charged at pH = 3.5, approach zero charge at the pI, and be negatively charged at pH 7.0. There would therefore be attractive protein-vesicle electrostatic interaction at pH 3.5 and repulsive interaction at pH 7.0, which is consistent with the observed vesicle binding at pH 3.5 and no binding at pH 7.0.

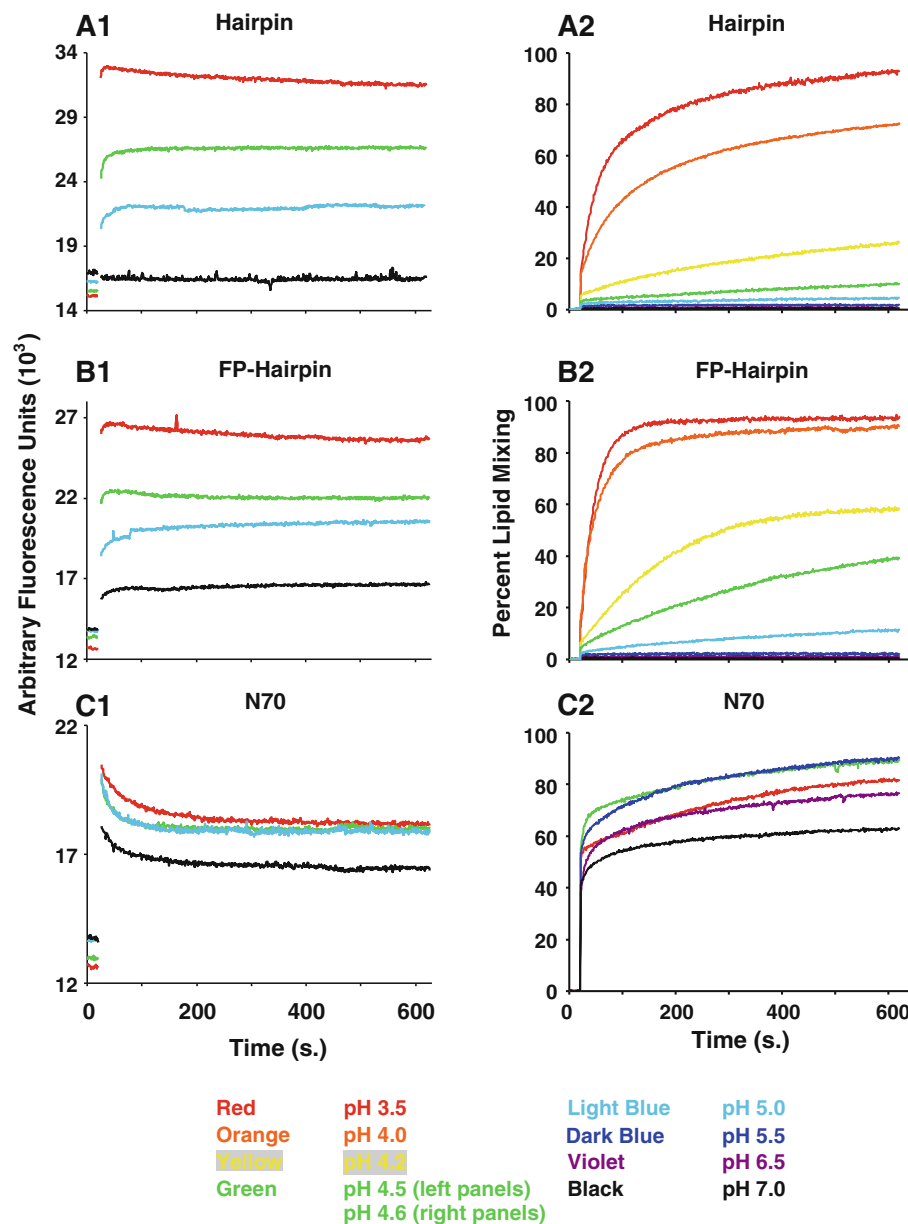


Fig. 4 pH-dependent membrane binding (**a1**, **b1**, **c1**) and vesicle fusion (**a2**, **b2**, **c2**) where **a**, **b**, and **c** correspond to Hairpin, FP-Hairpin, and N70, respectively. For each trace, a vesicle solution was prepared in 25 mM citrate buffer with [total lipid + cholesterol] \approx 230 μ M. At 20 s, protein was added with final [protein] = 1 μ M (Hairpin or FP-Hairpin) or 2 μ M (N70). For all panels, the *red*, *light blue*, and *black* traces correspond to pH = 3.5, 5.0, and 7.0, respectively. The *green* trace is pH = 4.5 (*left panels*) or 4.6 (*right panels*). *Orange*, *yellow*, *dark blue*, and *violet* traces in the

right panels correspond to pH = 4.0, 4.2, 5.5, and 6.5, respectively. The 525 nm fluorescence in the *left panels* is from *N*-dansyl-DOPE lipids in the vesicles. The excitation wavelength was 280 nm so that the increase in fluorescence after protein addition was due to energy transfer from tryptophan sidechains of the bound protein. Relative to **b1** and **c1**, slightly larger slitwidths were used in **a1**, which accounts for the higher baseline fluorescence in **a1** and fluorescence change due to protein within Förster distance. The lipid mixing assay of the *right panels* is described in the “Materials and methods” section

The pI of N70 is 11.5, and N70 is therefore likely positively charged in the pH 3.5–7.0 range with consequent attractive electrostatic interaction with the vesicles in this range. For N70 in the pH 3.5–7.0 range, it is therefore expected that both attractive electrostatic interaction and the FP hydrophobicity will contribute to approximately

pH-independent membrane binding, as was experimentally observed (Fig. 4c1). For FP-Hairpin with pI = 5.6, this model predicts attractive electrostatic and FP hydrophobic interaction with vesicles at pH 3.5 and repulsive electrostatic and attractive FP hydrophobic interaction at pH 7.0, which is consistent with significant binding at pH 3.5 and

lower but still substantial binding at pH 7.0, as was observed in Fig. 4b1.

Figures 3 and 4 provide some insight into the potentially competing processes of aggregation and membrane binding for Hairpin in the pH 4–6 range and for FP-Hairpin in the 4–7 range. For example, Hairpin extensively aggregates at pH 5.0 in the absence of vesicles, and Hairpin also binds significantly to vesicles at this pH. It seems improbable that very large Hairpin aggregates bind to vesicles, so it is likely that the binding rate of individual Hairpin SHB trimers to vesicles at pH 5.0 is at least comparable to the rate of aggregation of these trimers. Similar arguments apply to FP-Hairpin in the pH 4–7 range. For Hairpin, changing the pH from 5 to 7 results in dramatic decreases in both aggregation and binding so aggregation and binding are not necessarily inversely correlated. We note that although hydrophobic interactions underlie hyperthermostable SHB structure in Hairpin and FP-Hairpin, there is substantial evidence that the SHB does not unfold in either aggregated or membrane-associated protein (Peisajovich et al. 2003; Sackett et al. 2009, 2010).

pH-dependent vesicle fusion

Fusogenicity of the different constructs was probed using an intervesicle lipid mixing assay. We note that lipid mixing in HIV/host cell fusion is an earlier step associated with formation of the hemifusion diaphragm between the virus and cell. The N70 construct is a model of the N-terminal part of the early-stage PHI gp41 structure, whereas Hairpin and FP-Hairpin have the final-stage SHB structure. Earlier vesicle fusion studies have indicated that N70 and presumably the PHI are highly fusogenic, while there have been conflicting results about the fusogenicity of gp41 constructs with SHB structure. Some of these earlier lipid mixing studies were done at different pHs and motivated the present work on lipid mixing at pHs between 3.5 and 7.0 (Fig. 4 a2, b2, c2). N70 induced rapid and extensive vesicle fusion at all pHs in this range (panel c2), whereas Hairpin induced slower but still significant fusion at pH 3.5 with rapid loss in rate and extent of fusion with increasing pH and negligible fusogenicity for $\text{pH} \geq 5.0$ (panel a2). The fusogenicity of FP-Hairpin was also attenuated with increasing pH, but relative to Hairpin, FP-Hairpin induced measurably faster rate and extent of vesicle fusion in the pH 3.5–5.0 range with complete loss of fusogenicity at $\text{pH} \geq 5.5$ (panel b2). This result highlights the functional significance of the FP region. At low pH, SHBs fuse negatively charged vesicles and this charge was due to either a fraction of PS or PG lipid (Lev et al. 2009).

The effect of neutral pH on Hairpin or FP-Hairpin structures or interactions with the membrane might result

in irreversible loss of fusogenicity of the protein. Alternatively, pH reduction might reversibly change these protein properties back to the fusogenic ones. Figure 5 (red traces) supports the latter hypothesis with no fusion observed with incubation of protein + vesicles at pH 7.0 (treatment 1), while extensive fusion was triggered upon pH reduction to 3.3 (treatment 2). The black traces show that protein is required for pH-triggered fusion as lowering the pH of vesicle-only solution (treatment 1) did not induce vesicle fusion, while addition of protein to the low pH vesicle solution (treatment 2) resulted in vesicle fusion which was comparable to that observed with pH triggering in the red traces. In Fig. 5, the functional significance of the FP region of FP-Hairpin is highlighted by more extensive fusion of FP-Hairpin relative to Hairpin at pH 3.3, which correlates with the fusion data of Fig. 4a2, b2.

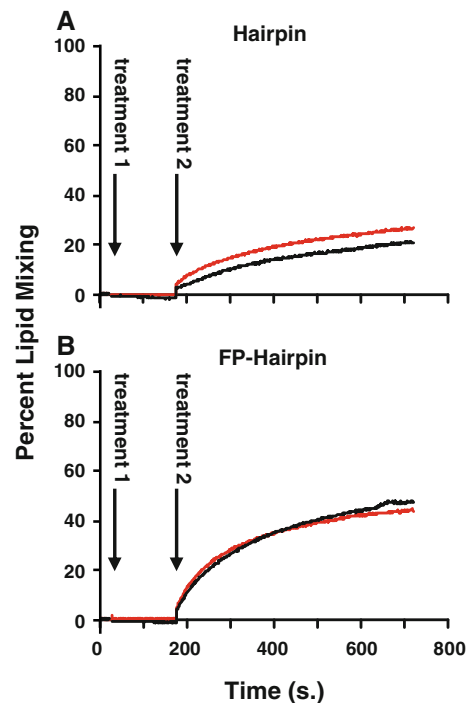


Fig. 5 pH-triggered vesicle fusion induced by **a** Hairpin or **b** FP-Hairpin. For each trace, a vesicle solution was prepared in 25 mM citrate buffer with $\text{pH} = 7.0$ and $[\text{total lipid} + \text{cholesterol}] \approx 230 \mu\text{M}$. At 20 s (treatment 1) in the red traces, an aliquot of protein was added and induced no fusion, whereas at 180 s (treatment 2), an aliquot of HCl reduced the solution pH to 3.3 and induced significant fusion. The pH 7.0 state of the protein was therefore not irreversibly nonfunctional. For the black traces, the order of addition was reversed so that treatments 1 and 2 correspond to addition of HCl and protein, respectively, and the data confirm that both protein and low pH are required to induce fusion. The final $[\text{protein}] = 0.33 \mu\text{M}$ and was threefold smaller than $[\text{protein}]$ in the Fig. 4 assays. For the Fig. 5 assay with sequential addition of protein followed by HCl, higher $[\text{protein}]$ induced formation of large vesicle aggregates which scattered radiation

Electrostatic contributions to aqueous solubility, membrane binding, and fusogenicity

Figure 6 provides a visual summary of much of the aqueous solubility, membrane binding, and fusogenicity data for the three constructs. Protein charge and electrostatic interactions help to explain much of the pH dependences of the experimental data. For example, the high solubilities of all three constructs at $\text{pH} \approx 3.5$ correlate with the overall positive molecular charges expected from the pIs and the consequent repulsive electrostatic intermolecular interaction. Aggregation was observed for each construct when the pH approached the pI and is explained by the reduction in both positive charge and intermolecular repulsion. For Hairpin with calculated $\text{pI} = 5.3$, aggregation was reduced and solubility was increased for $\text{pH} = 7.0$ and is explained by the significant negative charge on the SHB trimer and repulsive inter-trimer interaction.

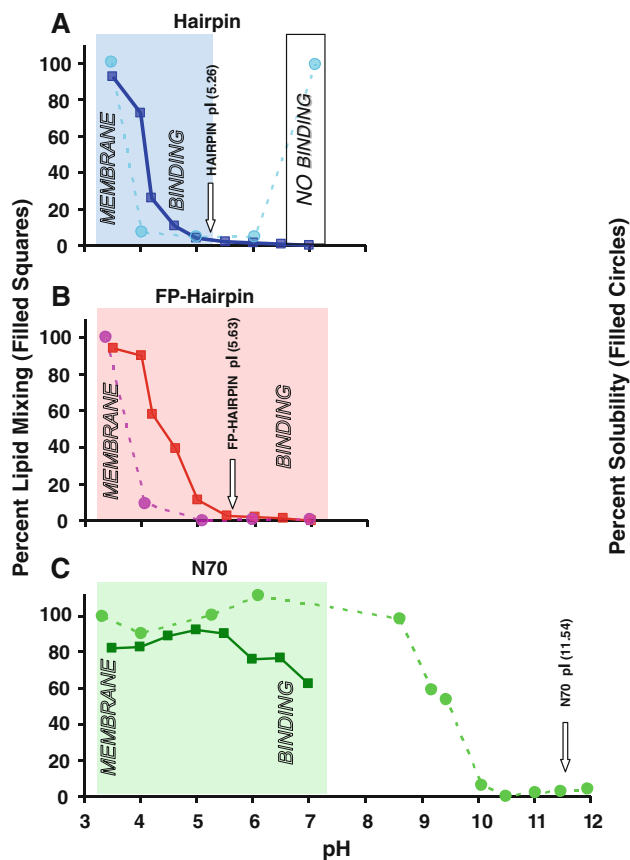


Fig. 6 Summary of pH-dependent data for **a** Hairpin, **b** FP-Hairpin, and **c** N70. The experimental solubility (relative to $40 \mu\text{M}$) and lipid mixing are shown as *circles* and *squares*, respectively, with *dashed* and *solid lines* drawn between data points. Each *shaded box* corresponds to the pH range of membrane binding (measured qualitatively) and the *dashed box* for Hairpin corresponds to the pH range without binding. The calculated pI for each construct is marked with an *arrow*

The role of electrostatics in membrane binding requires consideration of the 20% of the lipids in the vesicles that had negatively charged headgroups. High and no membrane binding of Hairpin were observed at $\text{pH} 3.5$ and 7.0 , respectively, and correlated with attractive and repulsive protein-vesicle electrostatic interaction expected for positively and negatively charged protein. Electrostatic repulsion also played a role in fusogenicity in at least two ways: (1) the corollary effect of no fusogenicity for cases in which there was no membrane binding, e.g., Hairpin at $\text{pH} 7.0$; and (2) inhibition of fusion even when there is protein binding by the FP as for FP-Hairpin at $\text{pH} 7.0$. We note that other studies have correlated the membrane insertion depth of the FP to FP-induced membrane perturbation and fusogenicity (Qiang et al. 2009). It may be that the electrostatic repulsion between the SHB and the vesicle draws the FP to the membrane surface with consequent reduction of fusogenicity.

Electrostatic attraction between the protein and the vesicle may also contribute to fusogenicity, e.g., for Hairpin at $\text{pH} 3.5$ (Walter et al. 1986). Relative to vesicles only, vesicles with bound Hairpin likely have smaller negative charge, which would reduce intervesicle repulsion and the fusion activation energy. The order of magnitude for this effect is calculated using the following approximations: (1) all Hairpin binds to the vesicles under the $\text{pH} 3.5$ assay conditions so that the Hairpin:POPG mol ratio is ~ 0.03 ; and (2) most Hairpin carboxyl groups are protonated at $\text{pH} 3.5$ so that the Hairpin molecular charge is $\sim +9e$ (Fig. 2d). The ratio of net negative charge of a vesicle with bound Hairpin to negative charge of vesicle only would then be ~ 0.7 . The ratio of corresponding intervesicle repulsion energies would be proportional to the square of the ratio of charges or ~ 0.5 . This effect may be larger if Hairpin binds to the vesicle surface (rather than transmembrane insertion) and is therefore close to the outer rather than inner leaflet lipids. If only outer leaflet POPG is considered, the charge ratio for (vesicle with Hairpin):(vesicle only) would be ~ 0.4 , and the corresponding intervesicle repulsion energy ratio would be ~ 0.2 . This latter calculation is important because lipid charges are localized in the headgroups and relative to inner leaflet lipids, outer leaflet lipids make a larger contribution to intervesicle repulsion.

Using similar arguments, FP-Hairpin bound to vesicles at $\text{pH} 3.5$ would reduce the electrostatic contribution to fusion activation energy, whereas at $\text{pH} 7.0$, it would increase this contribution and this increase could contribute to lack of fusogenicity despite the presence of the FP. The NHR region of N70 is positively charged at both $\text{pH} 3.5$ and 7.0 and is therefore likely to reduce electrostatic repulsion at both pHs. This hypothesis has been supported by observation of vesicle fusion at $\text{pH} 7.4$ induced by a

NHR peptide; however, we note the fusion extent is about an order of magnitude smaller than that of N70 for the same peptide:lipid ratio (Korazim et al. 2006). N70 contains the FP with antibody evidence that a significant fraction of N70 molecules are trimeric with topology shown in Fig. 2b (Sackett et al. 2006). Cross-linked FPs with trimeric topology are also highly fusogenic so the fusogenicity of N70 is likely due to a combination of trimeric FP topology and NHR/vesicle electrostatics (Qiang and Weliky 2009; Yang et al. 2004b). HIV/host cell fusion likely occurs near pH 7.0, and the most biologically significant results of the present work are the respective high and low fusogenicities of N70 and FP-Hairpin at pH 7.0. These results suggest that at least the lipid mixing step of fusion is catalyzed by the PHI state of gp41 (modeled by N70) and arrested by the SHB state (modeled by FP-Hairpin). These results are consistent with (1) data for gp41-induced fusion that correlate the PHI with hemifusion (Markosyan et al. 2003); (2) data showing inhibition of both gp41-induced fusion and HIV infection by SHB constructs (Lu et al. 1999; Shu et al. 2000); and (3) the reasonable hypotheses that fusion arrest by SHB reflects stabilization of the fused membrane and that this stabilization improves cell viability and is therefore advantageous to HIV for its replication.

Fusion of some enveloped viruses other than HIV (such as influenza) occurs in the acidified endosome at pH between 5 and 6 (Pan et al. 2010; White et al. 2008). This has motivated earlier studies that examined the pH dependence of vesicle fusion induced by influenza fusion protein constructs including the full ectodomain with fusion peptide (Curtis-Fisk et al. 2007; Epanand et al. 1999). There was rapid and extensive fusion at pH \approx 5 (similar to FP-Hairpin at pH 3.5) and little fusion at pH \approx 7 (similar to FP-Hairpin at pH 5.0). It would be worthwhile to consider the effect of pH-dependent electrostatics for these constructs. In some contrast, FP-Hairpin induced negligible vesicle fusion in the pH 5.5–7.0 range (Fig. 4b2), so we predict that the final SHB gp41 state would still be non-fusogenic under hypothetical (and to date unobserved) fusion of HIV in acidified endosomes.

The electrostatic effects observed in the present study will likely be modified by higher ionic strength. For example, addition of NaCl has resulted in much greater aggregation of FP-containing domains (Yang et al. 2001).

Oligomerization/aggregation of FP-Hairpin and fusogenicity

The minimum oligomerization state of Hairpin and FP-Hairpin is trimers due to the hyperthermostable SHB (Fig. 2). Antibody binding data are also consistent with trimer formation for a significant fraction of N70

molecules. The contribution of the FP trimeric topology to fusogenicity is evidenced by rapid and extensive N70-induced fusion and by the higher fusogenicity of FP-Hairpin relative to Hairpin. These data correlate with earlier studies showing 20-fold more rapid fusion and deeper membrane insertion of cross-linked FP trimers relative to non-cross-linked FPs (Qiang et al. 2009; Yang et al. 2004b). For FP-Hairpin at pH \geq 5.5, fusion enhancement by FP trimerization is completely counteracted by the SHB region, and this fusion inhibition may be due to (1) electrostatic repulsion between the SHB and the vesicle which pulls the FP trimer out of the membrane interior; and/or (2) increased inter-vesicle electrostatic repulsion because of the negative SHB charge.

In the absence of vesicles, trimers of FP-Hairpin aggregate under most pH conditions including the most biologically relevant pH \approx 7 (Fig. 6b). For the vesicle fusion as well as the membrane binding assays, nonaggregated FP-Hairpin at low pH was diluted into a vesicle solution at higher pH and aggregation of FP-Hairpin trimers could be concurrent with membrane binding and fusion. The mixture of aggregation state(s) of the bound FP-Hairpin trimers and their relative fusogenicities were not directly measured in our studies. However, as noted previously, membrane binding of FP-Hairpin trimers or small trimer aggregates probably occurs faster than extensive aggregation because (1) large protein aggregates likely do not bind to membranes; and (2) there was significant membrane binding for pH \geq 4 in which macroscopic aggregation was dominant in the absence of vesicles. By similar reasoning, detection of extensive vesicle fusion in the pH 4–5 range supports the fusogenicity of FP-Hairpin trimers or small trimer aggregates rather than large aggregates. This correlation between small oligomers/aggregates in aqueous solution and fusogenicity was also observed in an earlier study on different FP constructs which were either monomers, small aggregates, or large aggregates in aqueous solution prior to membrane binding and subsequent fusion (Yang et al. 2004a). Their extents of vesicle fusion were ordered as follows: large aggregates < monomers < small aggregates. These results have biological relevance because small aggregates of gp41 trimers have also been shown to be important in HIV/cell fusion (Magnus et al. 2009).

Reconciling results of earlier studies

This work was motivated by apparently conflicting reports in the literature about the vesicle fusogenicity of SHB gp41 constructs. Briefly, there was a report of very high fusion extents for SHB-only and FP + SHB constructs as well as reports of no fusion (Lev et al. 2009; Sackett et al. 2009, 2010). All of these studies used vesicles with a fraction of

negatively charged lipids, and the most obvious difference between the high- and no-fusion studies was the respective pHs of 3.0 and 7.2. An important result of the present work is detection of very rapid and extensive fusion for Hairpin (SHB) and FP-Hairpin (FP + SHB) constructs at pH 3.5 and no fusion at pH 7.0, thereby reconciling the apparent literature conflict. The change from positive protein charge at pH 3.5 to negative charge at pH 7.0 appears to be the underlying reason for much of the pH dependence, and this change was supported by formation of large protein aggregates in pH \approx pI aqueous solutions that did not contain vesicles.

The results of the present study likely hold for the full gp41 ectodomain with native loop and C-terminal membrane-proximal external region (MPER) because (1) a FP + SHB construct with native loop also didn't induce fusion of negatively charged vesicles at pH 7.4; and (2) the MPER adds just one more ionizable residue so that the full ectodomain has calculated pI \approx 6.3, which is close to the pI \approx 5.6 of FP-Hairpin (E. P. Vogel and D. P. Weliky, unpublished data). The present work does not resolve conflicting literature data about whether SHB and FP + SHB constructs induce fusion of vesicles without negatively charged lipids. There are studies reporting either no fusion or extensive fusion (Cheng et al. 2010; Lev et al. 2009). The latter study also provided data showing that relative to the SHB construct, the FP + SHB construct binds more strongly to membranes.

Conclusions

This work focused on measuring the pH dependences of HIV gp41 construct-induced fusion of vesicles where these vesicles contained a small mol fraction of negatively charged lipid (\sim 0.13 relative to total mol lipid + cholesterol). We wished to understand whether earlier reports of either extensive or no fusion induced by SHB gp41 constructs could be correlated to the respective pHs of 3.0 or 7.2 used in these studies. This pH dependence of fusogenicity was observed in the present study and resolved the apparently conflicting literature data. Corollary measurements of aqueous solubility and membrane binding support a model of positive SHB charge for pH \approx 3 and negative charge for pH \approx 7 with consequent respective attractive and repulsive electrostatic interaction with the vesicle. This difference in interaction is probably the major reason for the pH dependence of fusogenicity. A shorter N70 construct induced rapid vesicle fusion in the pH 3–8 range, which was due in part to retention of positive N70 charge and attractive interaction with vesicles over the entire pH range. N70 models part of the earlier-stage PHI state of gp41 during HIV/host cell fusion, whereas the FP-Hairpin models the final SHB gp41 state. Because HIV/host cell

fusion likely occurs with pH \approx 7, the data of the present study support a model of membrane perturbation and lipid mixing induced by early-stage PHI gp41 and membrane stabilization and fusion arrest by final-stage SHB gp41. This model is also supported by earlier studies of gp41-induced cell fusion and by inhibition of fusion and HIV infection by gp41 SHB constructs.

Other conclusions from this work include the following:

1. Membrane binding is a necessary but not sufficient condition for fusogenicity. “Necessary” is supported by the strong binding and fusogenicity of all constructs at pH 3.5, strong binding and fusogenicity of N70 at pH 7.0, and no binding and fusogenicity of Hairpin at pH 7.0. “Not sufficient” is supported by significant binding of FP-Hairpin at pH 7.0 without corollary fusogenicity.
2. The FP region and FP trimeric topology make significant contributions to membrane binding and fusogenicity as evidenced by comparison of data for FP-Hairpin relative to Hairpin. However, the fusogenicity of trimeric FP in FP-Hairpin can be completely inhibited by repulsive SHB/membrane interaction for pH \geq 5.5.
3. For Hairpin and FP-Hairpin, loss of solubility and fusogenicity at higher pHs can be completely reversed by lowering the pH, i.e., pH-induced changes in protein aggregation and structure are reversible.

Acknowledgments Dr. Lisa Lapidus is acknowledged for use of the fluorescence spectrometer and the MSU Mass Spectrometry facility is also acknowledged. The work was supported by NIH awards R01AI047153 to D.P.W. and F32AI080136 to K.S.

References

- Aloia RC, Tian H, Jensen FC (1993) Lipid composition and fluidity of the human immunodeficiency virus envelope and host cell plasma membranes. *Proc Natl Acad Sci USA* 90:5181–5185
- Bewley CA, Louis JM, Ghirlando R, Clore GM (2002) Design of a novel peptide inhibitor of HIV fusion that disrupts the internal trimeric coiled-coil of gp41. *J Biol Chem* 277:14238–14245
- Bjellqvist B, Hughes GJ, Pasquali C, Paquet N, Ravier F, Sanchez JC, Frutiger S, Hochstrasser D (1993) The focusing positions of polypeptides in immobilized pH gradients can be predicted from their amino acid sequences. *Electrophoresis* 14:1023–1031
- Brugger B, Glass B, Haberkant P, Leibrecht I, Wieland FT, Krausslich HG (2006) The HIV lipidome: a raft with an unusual composition. *Proc Natl Acad Sci USA* 103:2641–2646
- Caffrey M, Cai M, Kaufman J, Stahl SJ, Wingfield PT, Covell DG, Gronenborn AM, Clore GM (1998) Three-dimensional solution structure of the 44 kDa ectodomain of SIV gp41. *EMBO J* 17:4572–4584
- Callahan MK, Popernack PM, Tsutsui S, Truong L, Schlegel RA, Henderson AJ (2003) Phosphatidylserine on HIV envelope is a cofactor for infection of monocytic cells. *J Immunol* 170:4840–4845

- Center RJ, Leapman RD, Lebowitz J, Arthur LO, Earl PL, Moss B (2002) Oligomeric structure of the human immunodeficiency virus type 1 envelope protein on the virion surface. *J Virol* 76:7863–7867
- Chan DC, Kim PS (1998) HIV entry and its inhibition. *Cell* 93:681–684
- Chan DC, Fass D, Berger JM, Kim PS (1997) Core structure of gp41 from the HIV envelope glycoprotein. *Cell* 89:263–273
- Cheng SF, Chien MP, Lin CH, Chang CC, Lin CH, Liu YT, Chang DK (2010) The fusion peptide domain is the primary membrane-inserted region and enhances membrane interaction of the ectodomain of HIV-1 gp41. *Mol Membr Biol* 27:31–44
- Chernomordik LV, Zimmerberg J, Kozlov MM (2006) Membranes of the world unite! *J Cell Biol* 175:201–207
- Curtis-Fisk J, Preston C, Zheng ZX, Worden RM, Weliky DP (2007) Solid-state NMR structural measurements on the membrane-associated influenza fusion protein ectodomain. *J Am Chem Soc* 129:11320–11321
- Curtis-Fisk J, Spencer RM, Weliky DP (2008) Isotopically labeled expression in *E. coli*, purification, and refolding of the full ectodomain of the influenza virus membrane fusion protein. *Protein Expr Purif* 61:212–219
- Durell SR, Martin I, Ruyschaert JM, Shai Y, Blumenthal R (1997) What studies of fusion peptides tell us about viral envelope glycoprotein-mediated membrane fusion (review). *Mol Membr Biol* 14:97–112
- Eband RF, Macosko JC, Russell CJ, Shin YK, Eband RM (1999) The ectodomain of HA2 of influenza virus promotes rapid pH dependent membrane fusion. *J Mol Biol* 286:489–503
- Furuta RA, Wild CT, Weng Y, Weiss CD (1998) Capture of an early fusion-active conformation of HIV-1 gp41. *Nat Struct Biol* 5:276–279
- Gasteiger E, Hoogland C, Gattiker A, Duvaud S, Wilkins MR, Appel RD, Bairoch A (2005) Protein identification and analysis tools on the ExpASY server. In: Walker J (ed) *The proteomics protocols handbook*. Humana, Totowa, NJ
- Grewe C, Beck A, Gelderblom HR (1990) HIV: early virus-cell interactions. *J AIDS* 3:965–974
- Han X, Bushweller JH, Cafiso DS, Tamm LK (2001) Membrane structure and fusion-triggering conformational change of the fusion domain from influenza hemagglutinin. *Nat Struct Biol* 8:715–720
- Jaroniec CP, Kaufman JD, Stahl SJ, Viard M, Blumenthal R, Wingfield PT, Bax A (2005) Structure and dynamics of micelle-associated human immunodeficiency virus gp41 fusion domain. *Biochemistry* 44:16167–16180
- Johnson EC, Kent SB (2006) Insights into the mechanism and catalysis of the native chemical ligation reaction. *J Am Chem Soc* 128:6640–6646
- Jones PL, Korte T, Blumenthal R (1998) Conformational changes in cell surface HIV-1 envelope glycoproteins are triggered by cooperation between cell surface CD4 and co-receptors. *J Biol Chem* 273:404–409
- Korazim O, Sackett K, Shai Y (2006) Functional and structural characterization of HIV-1 gp41 ectodomain regions in phospholipid membranes suggests that the fusion-active conformation is extended. *J Mol Biol* 364:1103–1117
- Lev N, Fridmann-Sirkis Y, Blank L, Bitler A, Eband RF, Eband RM, Shai Y (2009) Conformational stability and membrane interaction of the full-length ectodomain of HIV-1 gp41: implication for mode of action. *Biochemistry* 48:3166–3175
- Li Y, Tamm LK (2007) Structure and plasticity of the human immunodeficiency virus gp41 fusion domain in lipid micelles and bilayers. *Biophys J* 93:876–885
- Lu M, Ji H, Shen S (1999) Subdomain folding and biological activity of the core structure from human immunodeficiency virus type 1 gp41: implications for viral membrane fusion. *J Virol* 73:4433–4438
- Macosko JC, Kim CH, Shin YK (1997) The membrane topology of the fusion peptide region of influenza hemagglutinin determined by spin-labeling EPR. *J Mol Biol* 267:1139–1148
- Magnus C, Rusert P, Bonhoeffer S, Trkola A, Regoes RR (2009) Estimating the stoichiometry of human immunodeficiency virus entry. *J Virol* 83:1523–1531
- Markosyan RM, Cohen FS, Melikyan GB (2003) HIV-1 envelope proteins complete their folding into six-helix bundles immediately after fusion pore formation. *Mol Biol Cell* 14:926–938
- McClure MO, Marsh M, Weiss RA (1988) Human immunodeficiency virus infection of CD4-bearing cells occurs by a pH-independent mechanism. *EMBO J* 7:513–518
- Miyauchi K, Kim Y, Latinovic O, Morozov V, Melikyan GB (2009) HIV enters cells via endocytosis and dynamin-dependent fusion with endosomes. *Cell* 137:433–444
- Nguyen DH, Hildreth JE (2000) Evidence for budding of human immunodeficiency virus type 1 selectively from glycolipid-enriched membrane lipid rafts. *J Virol* 74:3264–3272
- Pan JH, Lai CB, Scott WRP, Straus SK (2010) Synthetic fusion peptides of tick-borne encephalitis virus as models for membrane fusion. *Biochemistry* 49:287–296
- Peisajovich SG, Blank L, Eband RF, Eband RM, Shai Y (2003) On the interaction between gp41 and membranes: the immunodominant loop stabilizes gp41 helical hairpin conformation. *J Mol Biol* 326:1489–1501
- Pereira FB, Goni FM, Muga A, Nieva JL (1997) Permeabilization and fusion of uncharged lipid vesicles induced by the HIV-1 fusion peptide adopting an extended conformation: dose and sequence effects. *Biophys J* 73:1977–1986
- Qiang W, Weliky DP (2009) HIV fusion peptide and its cross-linked oligomers: efficient syntheses, significance of the trimer in fusion activity, correlation of beta strand conformation with membrane cholesterol, and proximity to lipid headgroups. *Biochemistry* 48:289–301
- Qiang W, Bodner ML, Weliky DP (2008) Solid-state NMR spectroscopy of human immunodeficiency virus fusion peptides associated with host-cell-like membranes: 2D correlation spectra and distance measurements support a fully extended conformation and models for specific antiparallel strand registries. *J Am Chem Soc* 130:5459–5471
- Qiang W, Sun Y, Weliky DP (2009) A strong correlation between fusogenicity and membrane insertion depth of the HIV fusion peptide. *Proc Natl Acad Sci USA* 106:15314–15319
- Reichert J, Grasnack D, Afonin S, Buerck J, Wadhvani P, Ulrich AS (2007) A critical evaluation of the conformational requirements of fusogenic peptides in membranes. *Eur Biophys J* 36:405–413
- Sackett K, Shai Y (2002) The HIV-1 gp41 N-terminal heptad repeat plays an essential role in membrane fusion. *Biochemistry* 41:4678–4685
- Sackett K, Shai Y (2003) How structure correlates to function for membrane associated HIV-1 gp41 constructs corresponding to the N-terminal half of the ectodomain. *J Mol Biol* 333:47–58
- Sackett K, Shai Y (2005) The HIV fusion peptide adopts intermolecular parallel beta-sheet structure in membranes when stabilized by the adjacent N-terminal heptad repeat: a ¹³C FTIR study. *J Mol Biol* 350:790–805
- Sackett K, Wexler-Cohen Y, Shai Y (2006) Characterization of the HIV N-terminal fusion peptide-containing region in context of key gp41 fusion conformations. *J Biol Chem* 281:21755–21762
- Sackett K, Nethercott MJ, Shai Y, Weliky DP (2009) Hairpin folding of HIV gp41 abrogates lipid mixing function at physiologic pH and inhibits lipid mixing by exposed gp41 constructs. *Biochemistry* 48:2714–2722

- Sackett K, Nethercott MJ, Eband RF, Eband RM, Kindra DR, Shai Y, Weliky DP (2010) Comparative analysis of membrane-associated fusion peptide secondary structure and lipid mixing function of HIV gp41 constructs that model the early pre-hairpin intermediate and final hairpin conformations. *J Mol Biol* 397:301–315
- Shu W, Liu J, Ji H, Radigen L, Jiang S, Lu M (2000) Helical interactions in the HIV-1 gp41 core reveal structural basis for the inhibitory activity of gp41 peptides. *Biochemistry* 39:1634–1642
- Stein BS, Gowda SD, Lifson JD, Penhallow RC, Bensch KG, Engleman EG (1987) pH-independent HIV entry into CD4-positive T-cells via virus envelope fusion to the plasma membrane. *Cell* 49:659–668
- Struck DK, Hoekstra D, Pagano RE (1981) Use of resonance energy transfer to monitor membrane fusion. *Biochemistry* 20:4093–4099
- Tan K, Liu J, Wang J, Shen S, Lu M (1997) Atomic structure of a thermostable subdomain of HIV-1 gp41. *Proc Natl Acad Sci USA* 94:12303–12308
- Tocanne JF, Teissie J (1990) Ionization of phospholipids and phospholipid-supported interfacial lateral diffusion of protons in membrane model systems. *Biochim Biophys Acta* 1031:111–142
- Tsui FC, Ojcius DM, Hubbell WL (1986) The intrinsic pK_a values for phosphatidylserine and phosphatidylethanolamine in phosphatidylcholine host bilayers. *Biophys J* 49:459–468
- Walter A, Steer CJ, Blumenthal R (1986) Polylysine induces pH-dependent fusion of acidic phospholipid vesicles—a model for polycation-induced fusion. *Biochim Biophys Acta* 861:319–330
- Weissenhorn W, Dessen A, Harrison SC, Skehel JJ, Wiley DC (1997) Atomic structure of the ectodomain from HIV-1 gp41. *Nature* 387:426–430
- White JM, Delos SE, Brecher M, Schornberg K (2008) Structures and mechanisms of viral membrane fusion proteins: multiple variations on a common theme. *Crit Rev Biochem Mol Biol* 43:189–219
- Winiski AP, McLaughlin AC, McDaniel RV, Eisenberg M, McLaughlin S (1986) An experimental test of the discreteness-of-charge effect in positive and negative lipid bilayers. *Biochemistry* 25:8206–8214
- Wu PG, Brand L (1994) Resonance energy transfer—methods and applications. *Anal Biochem* 218:1–13
- Yang J, Weliky DP (2003) Solid-state nuclear magnetic resonance evidence for parallel and antiparallel strand arrangements in the membrane-associated HIV-1 fusion peptide. *Biochemistry* 42:11879–11890
- Yang J, Gabrys CM, Weliky DP (2001) Solid-state nuclear magnetic resonance evidence for an extended beta strand conformation of the membrane-bound HIV-1 fusion peptide. *Biochemistry* 40:8126–8137
- Yang J, Prorok M, Castellino FJ, Weliky DP (2004a) Oligomeric beta-structure of the membrane-bound HIV-1 fusion peptide formed from soluble monomers. *Biophys J* 87:1951–1963
- Yang R, Prorok M, Castellino FJ, Weliky DP (2004b) A trimeric HIV-1 fusion peptide construct which does not self-associate in aqueous solution and which has 15-fold higher membrane fusion rate. *J Am Chem Soc* 126:14722–14723